Journal of Materials Research and Technology 35 (2025) 5782–5795

Contents lists available at ScienceDirect

Journal of Materials Research and Technology

journal homepage: www.elsevier.com/locate/jmrt

# Formation mechanism of ductile surface in ultrasonic elliptical vibration cutting of tungsten alloys basing on cemented carbide tools

Hao Su [a], Zhigang Dong [a], Yan Bao [a], Renke Kang [a], Sen Yin [b,*]

[a] State Key Laboratory of High-Performance Precision Manufacturing, Dalian University of Technology, Dalian 116024, PR China
[b] State Key Laboratory of Ultra-precision Machining Technology, Department of Industrial and Systems Engineering, The Hong Kong Polytechnic University, Kowloon, Hong Kong Special Administrative Region of China

ARTICLE INFO

Handling editor: M Meyers

*Keywords:*
Ultrasonic elliptical vibration cutting
Tungsten alloys
Material removal mechanism
Grain refinement
Dislocation density
Ductile surface generation

ABSTRACT

Tungsten alloys are widely employed in the fields of optics, medicine, and high-energy physics due to their exceptional physical properties. However, their inherent hardness, brittleness, and significant phase disparity present substantial challenges for precision & ultra-precision machining, including severe tool wear and surface defects. This research introduces ultrasonic elliptical vibration cutting (UEVC) with cemented carbide tools. It draws from the experience of UEVC of tungsten alloys with natural diamond tools in successfully achieving nanoscale surface. Comparative experiments involving cutting processes with and without the application of ultrasonic elliptical vibration were conducted to evaluate tool wear, chip formation, surface integrity, and the evolution of subsurface microstructures. The findings reveal that UEVC significantly suppresses tool wear and enables the formation of defect-free surfaces ($Sa$ = 115 nm) compared to conventional cutting. The subsurface features a uniform, nanocrystalline layer (~1000 nm in depth, with grain sizes ranging from 50 to 100 nm) and a broader dislocation distribution. This research corroborates the beneficial effects of ultrasonic vibrations in UEVC. It attributes the suppression of surface defects during the material removal process to the continuous ultrasonic impacts exerted by the tool. These impacts promote the proliferation, long-range motion, and interaction of dislocations, leading to a transition from brittle fracture to ductile removal modes, thereby supporting the prevailing "ultrasonic theory."

## 1. Introduction

95W-3.5Ni-1.5Fe alloys (referred to hereafter as tungsten alloys), are fabricated through liquid-phase sintering by embedding quasi-spherical single-crystal tungsten particles into a ductile Fe–Ni solid solution matrix [1,2]. Tungsten alloys exhibit remarkable physical properties, including high density (16.0–18.8 g/cm$^3$), high hardness, excellent high-temperature strength and creep resistance, as well as low deuterium-tritium retention rates and low sputtering yields. These attributes make tungsten alloys highly sought after in fields such as optics, medicine, and high-energy physics. Typical applications include optical lens molds, reaction chambers linings for large-scale high-energy physics experiments [3], and plasma-facing components such as divertor armor layers [4]. Consequently, tungsten alloys are recognized as strategically significant materials.

Despite their advantages, tungsten alloys pose substantial challenges in conventional machining due hardness (27–32 HRC) and brittleness (with a room-temperature elongation of only 0.01% for single-crystal tungsten particles) [5]. Material removal is predominantly governed by brittle fracture, resulting in severe tool wear and difficulties in achieving satisfactory surface quality. Furthermore, the bimodal mechanical properties of tungsten alloys (wherein the tungsten phase is hard and brittle, and the nickel-iron bonded phase is soft and viscous), lead to substantial disparities in material response. These differences induce alternating loads during machining, exacerbating tool wear and making tungsten alloys exceptionally difficult to process.

Ultrasonic elliptical vibration cutting (UEVC) superimposes ultrasonic elliptical vibration onto the tool tip to generate an elliptical motion trajectory. It has been widely employed to enhance the machinability of difficult-to-machine materials [6]. Numerous researchers have explored the use of UEVC combined with natural diamond tools to investigate ultra-precision machining of tungsten alloys, focusing on material removal mechanisms, surface formation dynamics, and process optimization. For instance, Pan et al. [7] developed a roughness prediction

* Corresponding author.
*E-mail address:* senyin@polyu.edu.hk (S. Yin).

https://doi.org/10.1016/j.jmrt.2025.02.229
Received 1 February 2025; Received in revised form 22 February 2025; Accepted 25 February 2025
Available online 25 February 2025

model for tungsten alloys in UEVC using convolutional neural networks. Yin et al. [8,9] conducted comparative studies on ductile surface generation mechanisms in UEVC of tungsten alloys by varying phase differences and ultrasonic vibration combinations, highlighting the role of strain rate. However, these studies primarily provided phenomenological analyses of surface roughness and hardness without delving into the microstructural evolution. Wang et al. [10–15] employed molecular dynamics simulations using LAMMPS to analyze the effects of cutting parameters, including rake angle and tool edge radius, on the ultra-precision machining of single-crystal tungsten. He concluded that the intermittent stress peaks during UEVC can exceed the activation thresholds of most slip systems in single-crystal tungsten, thereby addressing its low dislocation mobility. Bai et al. [16] investigated generation mechanisms of ductile surface in UEVC of tungsten alloys through a multi-scale coupling framework based on dislocation density. He identified the nucleation and migration of dislocations as the critical factors enabling ductile surface formation in UEVC of tungsten alloys. Collectively, these studies highlight the efficacy of UEVC with natural diamond tools in achieving ultra-precision machining of tungsten alloys.

However, natural diamond cutting tools, with edge radii ranging from 5 to 50 nm, are primarily suited for ultra-precision machining. Their high cost, limited cutting parameters (e.g., cutting speeds of 0.5–2 m/min, cutting depth of 1∼5 μm, and feed rates of 5∼15 μm/rev), and reliance on ultra-precision machine tools result in high machining costs, low efficiency, and restricted applicability to large-sized components. Conversely, tools made from cubic boron nitride (CBN), polycrystalline cubic boron nitride (PCBN), and cemented carbide offer greater adaptability, durability, and cost-effectiveness, are predominantly used for semi-precision and precision machining (The industry consensus is to require surface roughness between 0.8 μm and 0.16 μm with a tolerance grade of IT7 to IT5 for precision and 1.6 μm–0.8 μm with a tolerance grade of IT8 to IT7 for semi-precision machining). Many researchers have investigated precision machining of tungsten alloys using CBN, PCBN, and cemented carbide tools. Sreejith et al. [17] compared electrical discharge machining (EDM) with rough and finish turning using AlTiN-coated cemented carbide tools on a CNC turning center. The results indicated that even the best-performing finish turning yielded a surface roughness as high as 0.8 μm. Wang et al. [18] evaluated the cutting performance of different tools in turning of tungsten alloys, finding that TiAlN-coated cemented carbide tools demonstrated superior tool life (15 km) under optimized conditions. Mike et al. [19] conducted turning experiments on high-purity tungsten (W > 99.9%) using different tool materials, concluding that only PCD and PVD (TiAlN–TiSiN)-coated cemented carbide tools achieved satisfactory performance, albeit with limited surface roughness improvements (*Ra* = 1.1–1.7 μm). Nandam et al. [20] explored cutting experiments on tungsten alloys with a focus on cooling methods, introducing liquid nitrogen for forced cooling to mitigate the adverse effects of cutting heat on the tool. The results indicated that cryogenic cooling with liquid nitrogen effectively removed cutting heat from the machining zone, improving the machinability of tungsten alloys. Compared to conventional water-based cooling, this method reduced surface roughness by approximately 20% (from *Ra* 1.2 μm to *Ra* 1.0 μm), decreased cutting forces by about 50%, and extended tool life nearly threefold.

In summary, existing research on cutting tungsten alloys using cemented carbide tools is relatively limited and primarily focuses on two approaches: exploring different tool materials and controlling cutting temperatures. Nevertheless, the issues of high cutting forces/heat, severe tool wear, and the inability to further enhance surface machining quality remain unresolved. Some researchers propose that the impact effect generated by ultrasonic elliptical vibration combined with natural diamond tools induces localized high pressure in the cutting zone. This effect is attributed to the extremely sharp cutting edge of natural diamond tools (approximately 5∼50 nm), which creates an exceptionally small tool-workpiece contact area and leads to localized high pressure. These conditions significantly influence the material removal mechanism of tungsten alloys by inducing microstructural evolution [9,21,22]. This insight prompts us to consider: the cemented carbide tools, which lack such a small tool-workpiece contact area in cutting process, how would the introduction of ultrasonic elliptical vibration affect the material removal mechanism and the microstructural evolution of tungsten alloys? This question is critical for the assembly precision and service life of tungsten alloy components in various application scenarios. However, the underlying mechanisms remain unknown. Hence, this study aims to draw inspiration from the remarkable effects of UEVC observed in machining tungsten alloys with natural diamond tools, to investigate the application of UEVC using cemented carbide tools. While confirming the feasibility of UEVC tungsten alloys with cemented carbide tools, an attempt was made to elucidate the material removal mechanism and surface formation mechanism. It will help fill the gap in the field of UEVC tungsten alloys for precision machining. It is worth noting that this research may inversely contribute to the theoretical development of UEVC tungsten alloys for ultra-precision machining.

This investigation integrates UEVC technology with cemented carbide tools. An investigation was undertaken to conduct a comparative analysis of tool wear, surface integrity, chip formation, and subsurface microstructure during the machining of tungsten alloys, with and without the application of ultrasonic elliptical vibration. The results reveal the material removal mechanism and surface formation process of UEVC using cemented carbide tools. This methodology markedly enhances the precision and semi-precision machining capabilities of tungsten alloys. Furthermore, the research offers a valuable reference for the precision and semi-precision machining of other difficult-to-machine metallic materials, providing significant insights for advancing and expanding the industrial implementation of UEVC technology.

## 2. Experiments

The experimental setup for UEVC of tungsten alloys is shown in Fig. 1. The machining was performed on a three-axis ultra-precision single-point diamond turning machine, which consists of a spindle/C-axis, X-axis, and Z-axis. The UEVC system, independently developed, operates at an frequency of 27 kHz with a peak-to-peak amplitude of 4 μm. The workpiece material is provided by Beijing Antai Technology Co, Ltd, China. The sample geometry is a cylinder with a diameter of 15 mm and a height of 5 mm. The mechanical performance parameters of tungsten alloys are summarized in Table 1.

To investigate the surface quality, chip formation, microstructure, and cutting force variations under both UEVC and CC conditions, experiments were conducted in two groups. For CC, the ultrasonic power was deactivated, with the UEVC device functioning solely as a tool holder. The specific machining parameters are detailed in Table 2 (The experimental parameters were chosen with reference to the studies of machining of tungsten alloys by cemented carbide tools and UEVC of tungsten alloys with natural diamond tools [18,23]). The cutting tool used was a TiAlN-coated cemented carbide tool (KC5010) manufactured by Kennametal, USA. The tool features a nose radius of 0.4 mm, an edge radius of 20 (±5) μm, a rake angle of 0°, and a flank angle of +15°.

The surface roughness of the machined samples was measured using a Surface Optical Profiler (SOP, NewView 9000, Zygo Corporation, USA). The surface morphology and chips were characterized using a Scanning Electron Microscope (SEM, SU5000, Hitachi, Japan). The cross-sectional microstructure evolution of the samples was analyzed via Electron Backscatter Diffraction (EBSD). Samples for Transmission Electron Microscopy (TEM, FEI Tecnai F20 200 kV) observation were prepared using a Focused Ion Beam (FIB, Helios 5CX). A dynamometer (kistler, Switzerland) was used for the cutting process cutting force acquisition with a sampling frequency of 90 kHz. Three measurements were taken, and the average value was calculated.

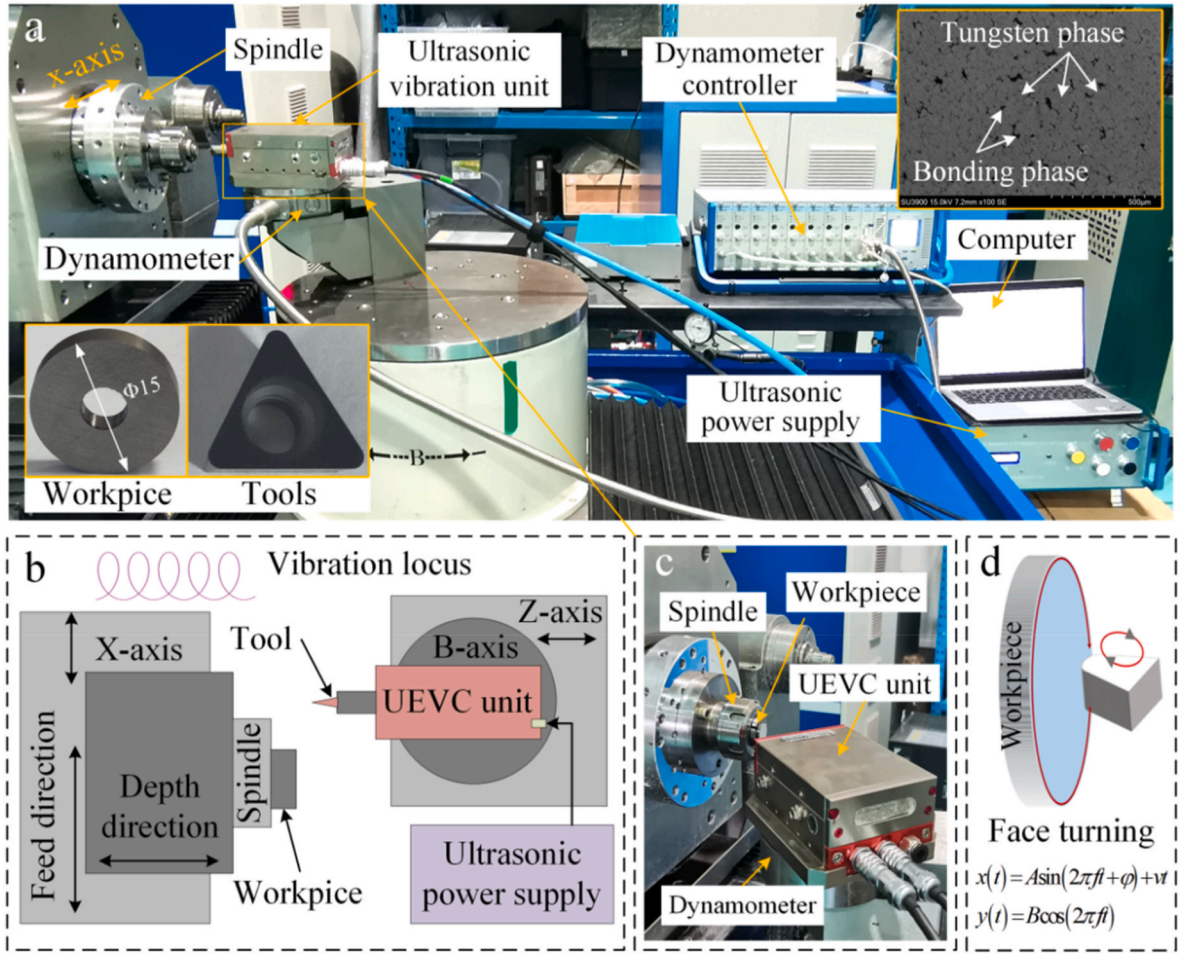


**Fig. 1.** Cutting experiment site and principle schematic: (a) Experimental site, (b) Schematic of cutting process, (c) Principle schematic of cutting process, (d) Cutting mode.

**Table 1**
Mechanical performance parameters of tungsten alloys.

| Items | Tungsten alloys |
|---|---|
| Match | 95 W-3.5Ni-1.5Fe |
| Heat treatment | Sintering |
| Density/(g/cm$^3$) | 18.10 ± 0.15 |
| Elongation (%) | 8~22 |
| Tensile strength/MPa | 800~1100 |
| Hardness/HRC | 27~32 |

**Table 2**
Experimental parameters.

| Items | UEVC | CC |
|---|---|---|
| Cutting speed $v_s$/m·min$^{-1}$ | 20 | 20 |
| Nominal cutting depth $a_p$/μm | 15 | 15 |
| Feed rate $f_r$/μm·r$^{-1}$ | 20 | 20 |
| Ultrasonic amplitude $A_X$/μm | 4 | 0 |
| Ultrasonic amplitude $A_Y$/μm | 4 | 0 |
| Frequency $f$/kHz | 27 | 0 |
| Cooling conditions | Alcohol | Alcohol |
| Tool material | Tungsten carbide | Tungsten carbide |

## 3. Results and analysis of experiments

### 3.1. Tool wear

The wear morphology of the cemented carbide tool is presented in Fig. 2. Fig. 2 (a) depicts the worn region of cemented carbide tool in CC. As observed in Fig. 2 (b), the tool exhibited significant wear, predominantly on the flank face. The worn area appeared relatively flat, with minor scratches and a small amount of adhesion on the surface. Notably, no "thin-to-thick" transitional features characterized of the coating layer were observed at the edges of the worn region. The predominant wear mechanism in CC was identified as mechanical abrasion, mainly attributed to the presence of hard tungsten phases in tungsten alloys. The scratches at the edges of the wear area further confirmed this observation.

Energy dispersive spectroscopy (EDS) analysis revealed variations in the content of the original elements W, N, and C within the wear region, as shown in Fig. 2 (c). Additionally, elements from the workpiece material, such as Ni and Fe, as well as O from the ambient environment, were detected. The absence of coating elements (e.g., Ti and N) on the worn surface indicated that the coating had been completely removed, rendering it ineffective in protecting the tool. While W is a base material element of the tool, it may also originate from the diffusion of tungsten alloys as evidenced by the presence of small amounts of Ni and Fe, further supporting the occurrence of diffusion wear during the cutting process. The presence of oxygen was attributed to oxidation wear, which occurred due to the oxidation of the tool material during cutting. The

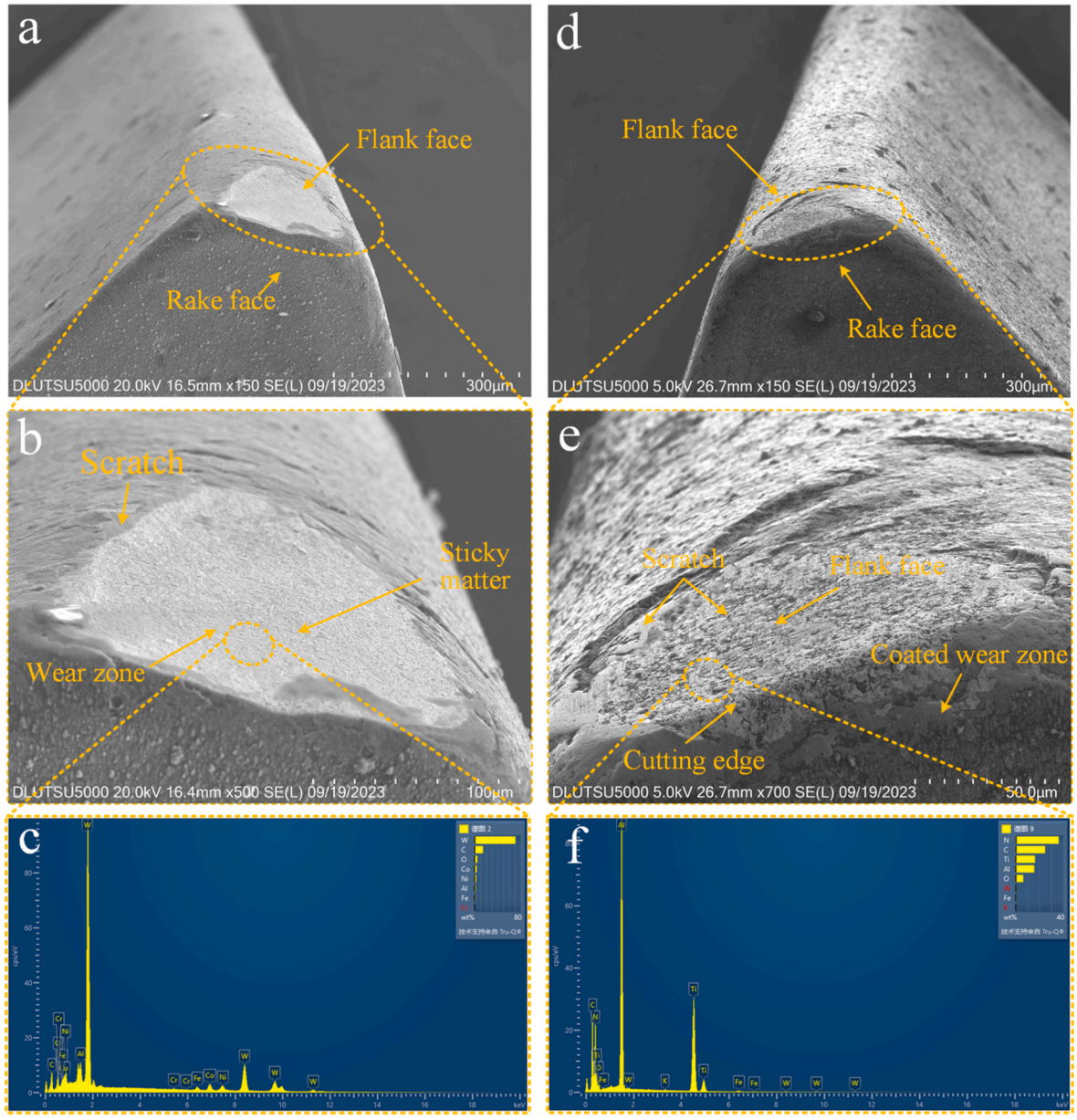


**Fig. 2.** Topography of tool wear: (a) SEM image of worn-out cutting tool by CC: (b) Magnified view of (a), (c) EDS analysis of cutting tools in CC, (d) SEM image of worn-out cutting tool by UEVC, (e) Magnified view of (c), (f) EDS analysis of cutting tools in UEVC.

oxidation initiation temperature for cemented carbide was approximately 300 °C, and previous studies indicated that cutting temperatures under these conditions can reach up to 375 °C, leading to oxidation of the tool material. The resulting oxidation reactions reduced the hardness of the tool, accelerating mechanical wear. In summary, the predominant wear mechanisms of TiAlN-coated cemented carbide tools in CC were mechanical abrasion, accompanied by diffusion wear and oxidation wear.

Fig. 2 (d) depicts the worn region of the cemented carbide tool under UEVC. It was evident that the tool's overall geometry remains relatively intact, with no observable fracturing or chipping of the cutting edge. Nevertheless, localized coating wear and spalling can be detected. A higher-magnification view in Fig. 2 (e) the sequential presence of the tool coating, the coating wear zone, and the underlying substrate one can be clearly observed. Elemental analysis in Fig. 2 (f) indicated that the main elements in the worn region were N, Ti, and Al—typical constituents of the coating—indicating that the coating has not been completely breached. In conjunction with the observed wear morphology, this finding indicated that UEVC effectively suppressed tool wear. This effect is primarily attributed to the unique micro-removal and friction reversal characteristics introduced by UEVC, which reduce friction and inhibit material adhesion, thus mitigating tool wear and extending tool life. The smooth coating wear band and the scratch marks observed within the worn zone indicate that mechanical friction remains the dominant wear mechanism. Moreover, the presence of oxygen in the EDS analysis confirms that oxidative wear still occurs.

Additionally, the reduction in cutting forces in UEVC is another critical factor in mitigating tool wear. As illustrated in Fig. 3(a–b), which presents the time-domain signals of the cutting forces, and Fig. 3 (c), which compares their average values (where *Fx* is the feed-direction force, *Fy* is the cutting force along cutting depth, and *Fz* is the main cutting force along cutting direction), UEVC exhibits markedly lower cutting forces compared to CC—most notably along the cutting direction, where the average cutting force in UEVC (0.466 N) is merely one-third of that in CC (1.337 N). This significant reduction in cutting force evidently diminished mechanical frictional wear on the tool.

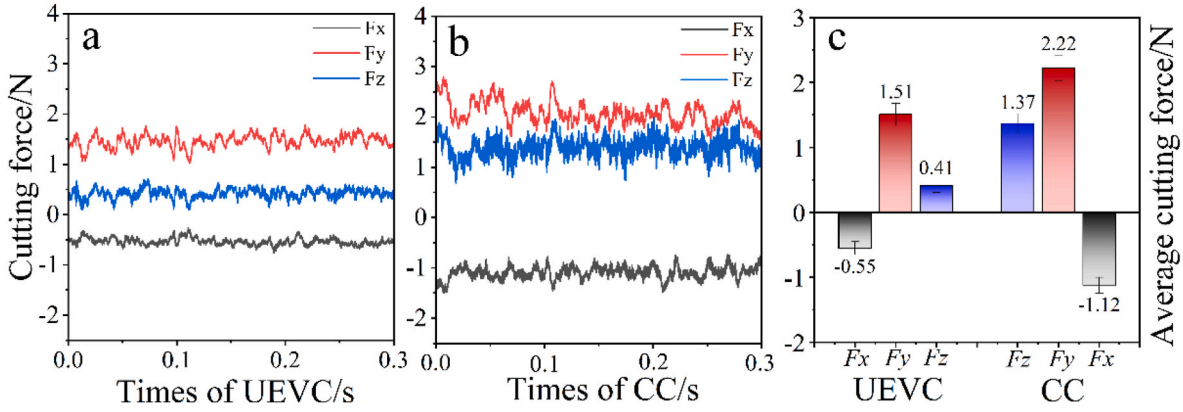


**Fig. 3.** Comparison of cutting forces between UEVC and CC: (a) Time-domain of cutting force in UEVC, (b) Time-domain of cutting force in CC, (c) Average cutting force.

### 3.2. Surface morphology

As illustrated in Fig. 4, the surface morphologies of workpieces machined by CC and UEVC exhibit marked differences.The characterization of material removal modes was conducted by examining the type, quantity, and spatial distribution of surface damage. In Fig. 4(a–c) the appearance of "scale-like" folded material, microcracks, and tungsten-phase spalling indicates that the surfaces machined by CC predominantly undergo brittle or semi-brittle removal. Under the compressive action of the tool, tungsten particles—limited by their intrinsic material properties—failed to undergo plastic deformation. Once energy accumulates beyond the fracture threshold, the release occurs through brittle fracture mechanisms, manifested as microcracks and material spalling. Conversely, the surfaces depicted in Fig. 4(d) and (e), machined by UEVC, feature a highly regular wavelike pattern (attributable to the geometric trajectory of ultrasonic elliptical vibration) and are essentially defect-free. The formation of defect-free surfaces depends on the enhancement of material deformation plasticity and suppression of brittle fracture during material removal, Further, this can be attributed to the generation of a large range of high-density dislocations and ordered nanofine crystalline layers induced by ultrasonic elliptical vibrations. This morphology reflects a ductile removal characteristic, distinguishing UEVC from the brittle or semi-brittle modes in CC.

Fig. 5 presents 3D surface profiles of the machined samples. Upon examining the residual cutting height and surface defects, further insights into the material removal modes for each machining method could be gained. Fig. 5 (a), numerous pits (blue spots, Sa ≈300 nm, which is significantly lower than that of 290 nm for CC.) resulting from material fragmentation was observed, reaffirming the presence of brittle fracture during the CC. By contrast, Fig. 5 (d) reveals that the quantity and depth of pits on machined surface in UEVC are substantially reduced, yielding a smoother surface in the cutting direction (Sa ≈117 nm) and more regular feed marks. These features suggest that material removal in UEVC may occurred in a ductile or partially ductile regime.

### 3.3. Chip and subsurface morphology analysis

Section 3.2 characterization results confirm that UEVC with cemented carbide tools can achieve better surface quality of tungsten alloys. However, relying solely on surface quality improvements to substantiate a transition in the material removal mode remains

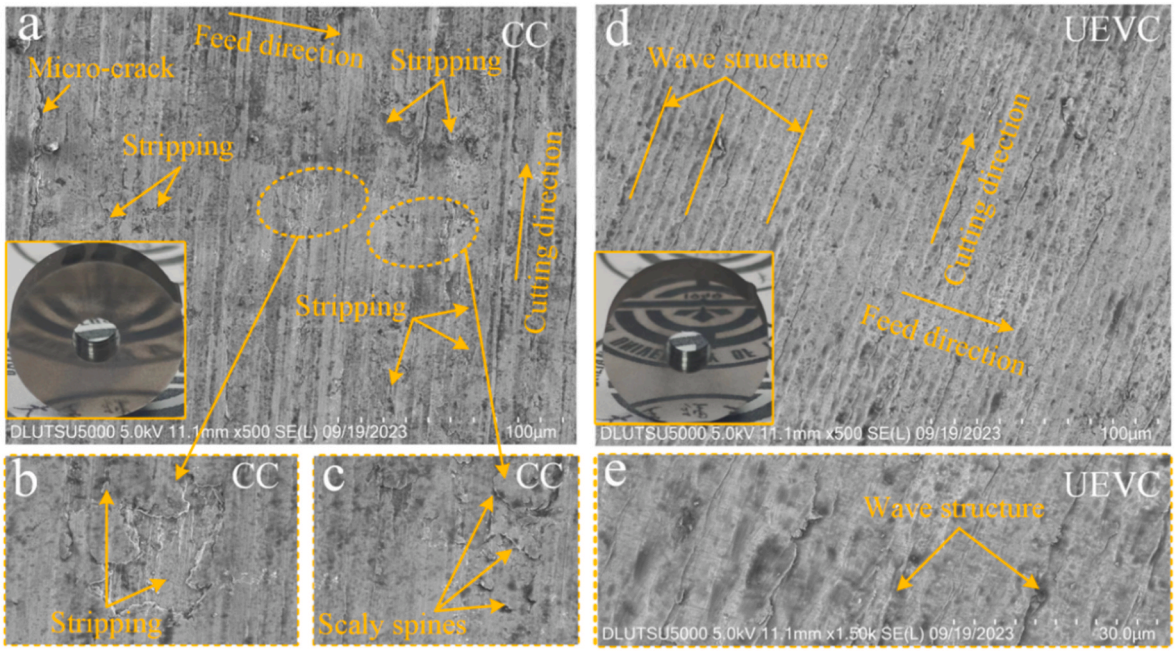


**Fig. 4.** SEM images of processed surface morphology of tungsten alloys: (a)–(c) CC, (g) & (j) UEVC.

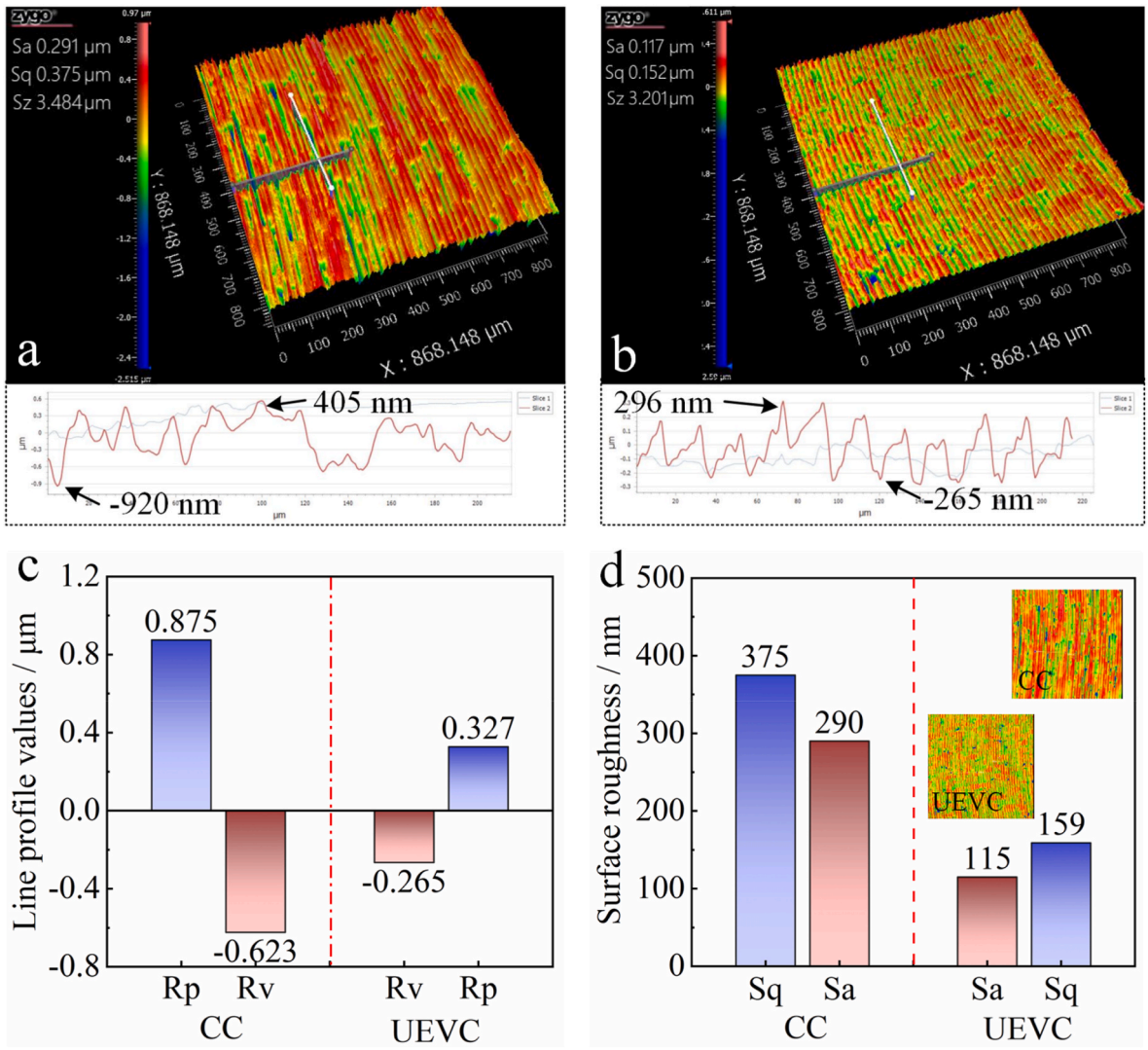


**Fig. 5.** 3D profiles of machined surface between UEVC and CC: (a) machined surface of CC; (b) machined surface of UEVC, (c)(d) Comparison of surface characteristics.

inconclusive. This is because it could also be the interference between the tool and the material, leading to slight plastic deformation. This deformation likely smooths over the brittle fracture marks, while simultaneously creating a wavelike structure on the surface. To further investigate the technical feasibility of using cemented carbide tools in UEVC of tungsten alloys, it is essential to analyze the chips formation during the cutting process and the subsurface morphology of the machined workpieces. Specifically, conductive adhesive tape was used to collect the chips, which are then observed using SEM.

In comparison to the intermittent quasi-shear state observed in the chip formation process during CC, UEVC undoubtedly leads to a continuous shear state. As shown in Fig. 6, the chips formed in CC was fragmented, with lengths ranging from 50 to 200 μm. The bottom of the chips exhibits plastic deformation and surface tearing along the chip flow direction. These features are attributed to the strong compression and high friction between the chip base and the tool's rake face. In contrast, as illustrated in Fig. 7, UEVC significantly increases the chip length (with chips reaching lengths of 500–2000 μm, which is 3–10 times greater than those in CC). The bottom of chips also shows noticeable plastic deformation but without significant tearing damage, indicating that the material removal process is dominated by shear deformation in a stable ductile removal mode. The increase in chip length undoubtedly indicates an increase in the plastic deformability of the material during UEVC tungsten alloys, which has been attributed to the ultrasonic vibration promoting the proliferation and migration of dislocations, thus increasing the plasticity of the material (please refer to the subsequent discussion section for the theoretical basis).

Similar to the chip analysis reflecting the removal process, the sub-surface microstructure further characterizes the material removal mode. As shown in Fig. 8(a–c), the subsurface of CC exhibits prominent microcracks, corresponding to the brittle fracture phenomenon commonly observed in CC. This suggests that the material removal mode in CC involves an interplay between intermittent shear and brittle fracture. In contrast, as shown in Fig. 8(d) and (e), no microcracks are observed in the subsurface of UEVC sample (Region A primarily consists of compressed tungsten particles and Ni–Fe binding phase, with slender black gaps corresponding to compressed Ni–Fe binding phases, not microcracks). Therefore, the material removal mode in UEVC was determined to be continuous plastic shear removal. In summary, the results of the chip morphology (length, upper and lower surface morphology) and sub-surface micro-morphological observations confirm the change in the material removal pattern under the different cutting modes, which is responsible for the high surface quality of UEVC.

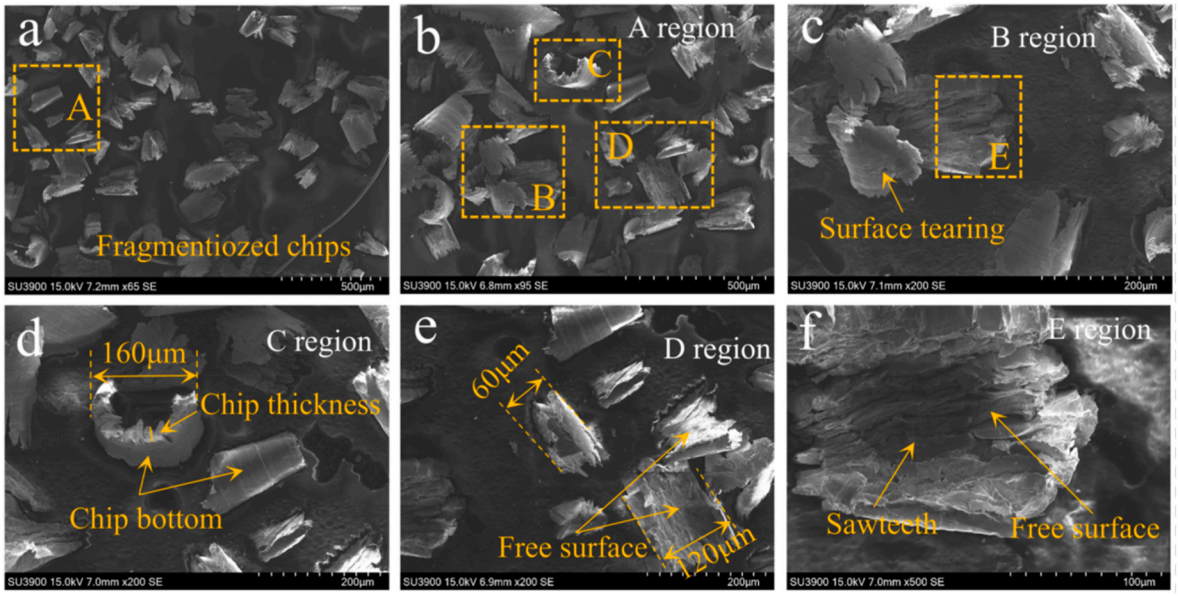


**Fig. 6.** Chip morphology of CC: (a) Overview of chip morphology, (b) Partially enlarged view of (a), (c) Damage on the chip bottom and chip free surface, (d) cross section of chip morphology and chip bottom, (e) Chip length, (f) Chip free surface and partial sawtooth morphology.

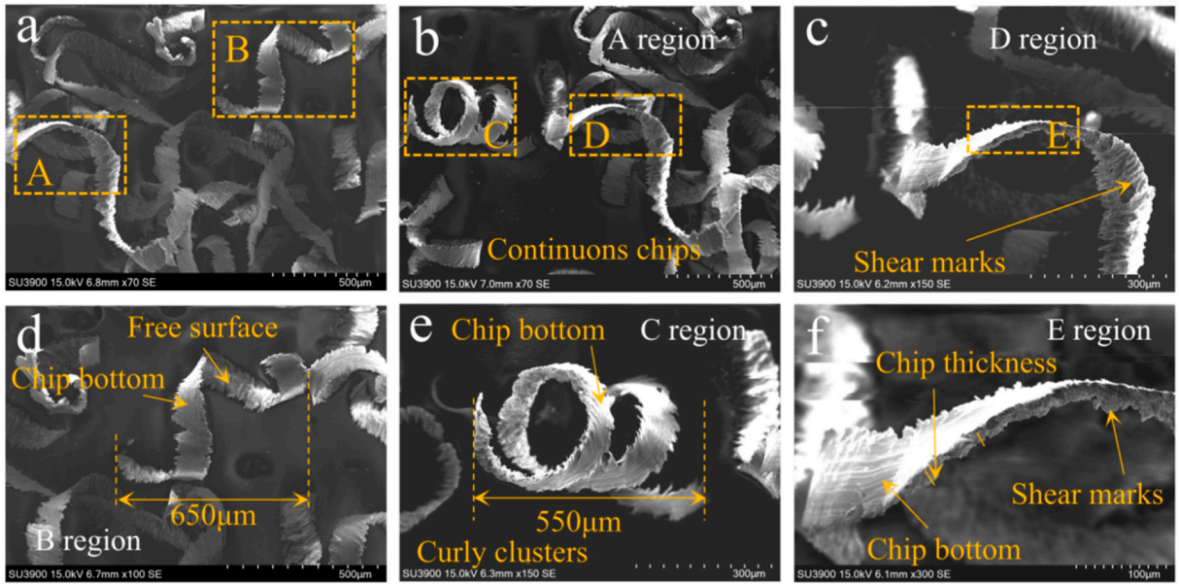


**Fig. 7.** Chip morphology of UEVC: (a) Overview of chip morphology, (b) Partially enlarged view of (a), (c) Cross section of chip morphology and chip free surface, (d) Chip bottom and chip length, (e) Chip length, (f) cross section of chip morphology.

### *3.4. Subsurface EBSD analysis*

Macroscopically, tungsten alloys exhibit degree of plasticity (tensile elongations ranging from 8% to 20%) [12,24]. However, this plasticity primarily arises from deformation in the Ni–Fe binder phase. By contrast, tungsten particles themselves possess pronounced hardness and brittleness, which underlies the fundamental challenges in machining tungsten alloys. Accordingly, this research focuses on the crystal structure evolution of single-crystal tungsten particles, excluding the influence of the binder phase or the interphase boundaries.

Fig. 9 presents the subsurface dislocation distributions in tungsten alloys. Although the maximum dislocation density does not differ significantly between the two cutting processes. Closer inspection reveals that, dislocations was confined to a depth of approximately 5 μm beneath the surface in CC. In contrast, under UEVC, the dislocation-affected region extends to approximately 25 μm. This observation aligns with K.W. Siu's [25] conclusion that "superimposed ultrasonic vibrations promote longer-range dislocation motion", thereby providing theoretical support for subsequent investigations into the transition mechanisms of tungsten alloy material removal.

Fig. 10 presents Inverse Pole Figure (IPF) maps illustrating the local morphology and grain size of the subsurface region of tungsten alloys specimens. As shown in Fig. 10(a) and (b), surface morphology of CC exhibits a flowing, gently sloping mountainous structure, and the grain refinement within the subsurface region is not notably pronounced, with a limited affected layer thickness. This limited grain refinement is primarily attributed to the substantial energy dissipation caused by brittle fracture, such as transgranular cleavage fractures, occurring in the single-crystal tungsten particles. These fracture modes consume significant energy, thereby reducing the efficacy of grain refinement in the

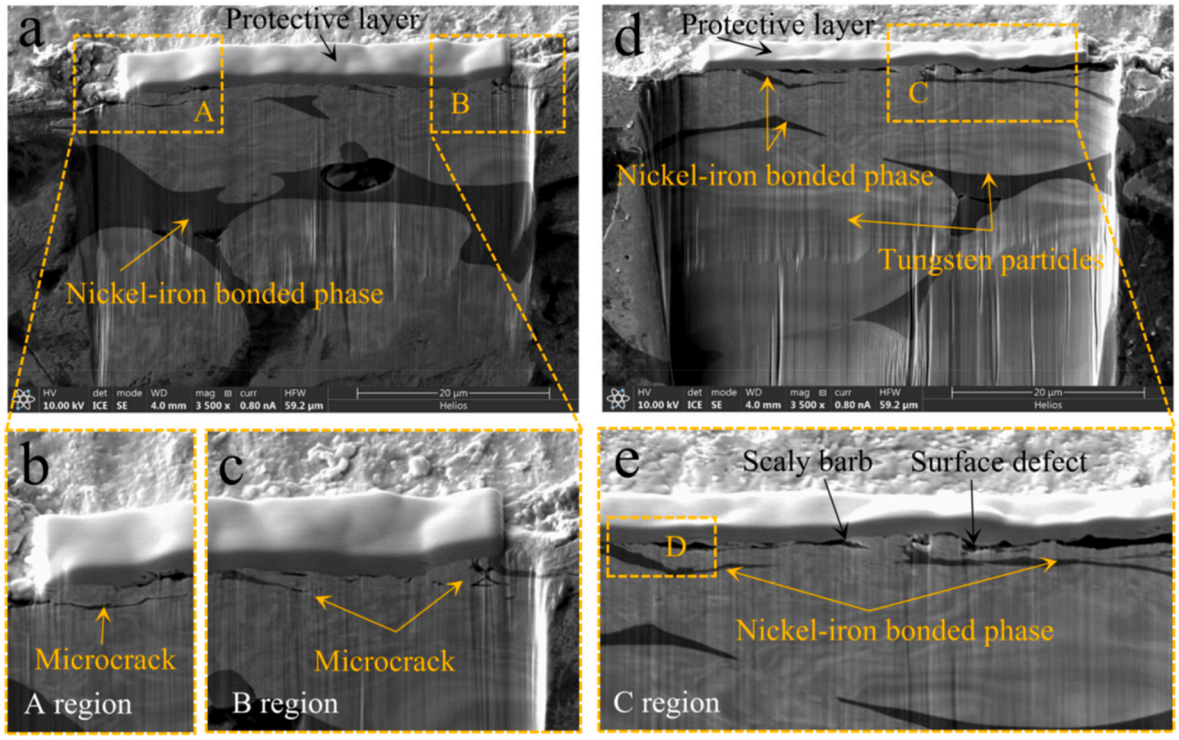


**Fig. 8.** Sub-surface micrographs. (a) Sub-surface micro-morphology of CC: (b) Enlarged view of sub-surface microcracks on CC, (c) Sub-surface micro-morphology of UEVC, (d) Localized enlargement of the subsurface morphology of UEVC.

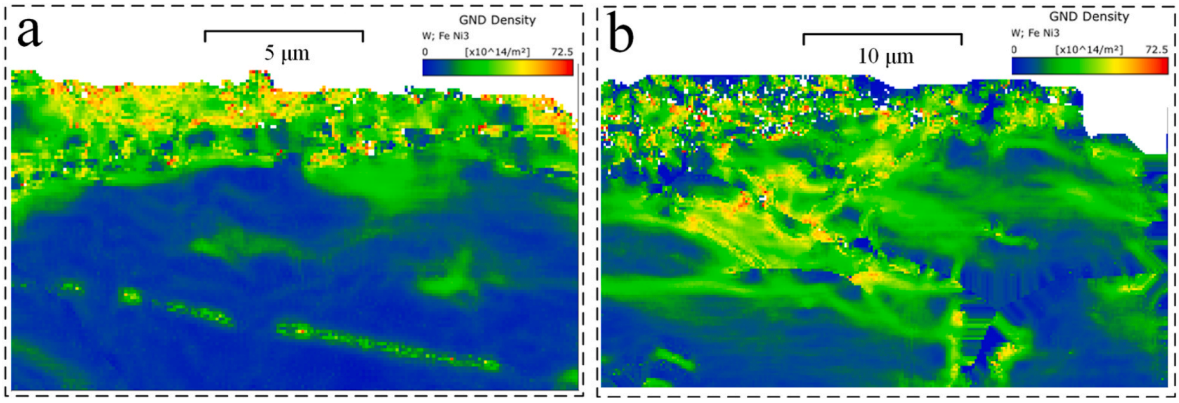


**Fig. 9.** Distribution of sub-surface dislocations by CC and UEVC: (a) CC, (b) UEVC.

subsurface region.

In contrast, the surface generated by UEVC depicted in Fig. 10, was markedly smoother and devoid of the mountainous structures observed in CC. Simultaneously, UEVC subsurface exhibits a uniform, consistent, and orderly grain refinement layer (depth of approximately 5 μm), where the average grain size was reduced to 50–500 nm (original single-crystal tungsten particles diameters of 40 μm). Notably, the refined grain layer exhibits a gradient distribution, with grain diameters in the topmost surface layer ranging from approximately 50 to 100 nm. The grain boundaries within the refined layer are predominantly formed by dislocation walls induced by ultrasonic vibrations. These dislocation walls undergo processes such as migration, aggregation, and annihilation of numerous dislocations, leading to the transformation of high-density dislocation walls into subgrain boundaries. Ultimately, dynamic recrystallization occurs, completing the grain refinement of tungsten [26–28]. Additionally, ultrasonic vibration introduces a substantial number of dislocations while inducing localized plastic deformation. This results in pre-damage within the first and second deformation zones of the material, facilitating ductile material removal and enhancing the cutting performance of tungsten alloys.

### 3.5. TEM analysis

The TEM bright-field images in Figs. 11 and 12 reveal subsurface microstructures under different machining conditions, providing insight into dislocation characteristics and grain boundary distribution. The micrographs validate previous analyses, showing a significant increase in dislocation density and the formation of an ultrafine-grained (UFG) layer near the surface, with a thickness of 300~1000 nm.

Fig. 11 illustrates the subsurface microstructure of machined samples in CC. Parallel and intermittently persistent slip bands (PSBs) containing tangled dislocation configurations are evident, which contribute to the initiation and propagation of microcracks within grain interiors. Fig. 11 (c) and (d) provide enhanced details of specific regions in Fig. 11 (b). In

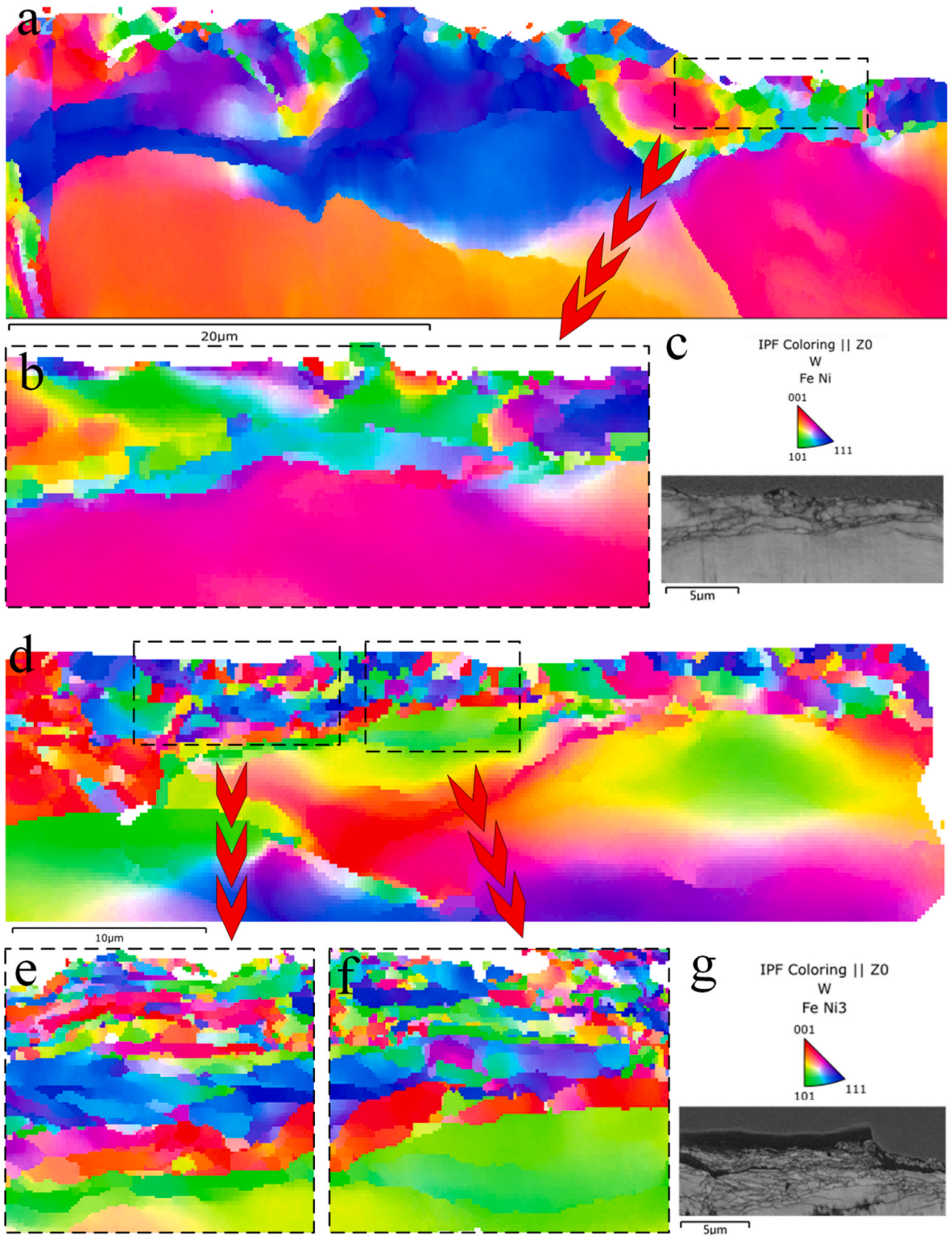


**Fig. 10.** EBSD IPF maps of machined surface by CC and UEVC: (a)–(c) CC, (d)–(g) UEVC.

addition to the refined grains formed through dynamic recrystallization, twin structures and tightly bonded fragmented particles are observed (The boundaries of these particles appear thin and indistinct, which prevents them from being conclusively classified as refined grains).

Fig. 12 illustrates the subsurface microstructure of UEVC samples. The micrographs reveal distinct curved grain boundaries, interwoven dislocations, well-defined ultrafine grains, and the presence of twins. In addition, twin structures were present, although their density is relatively low. This observation indicates that dislocation slip is the dominant deformation mechanism during UEVC of tungsten alloys. The UFG layer in UEVC samples is approximately three times thicker than that in CC, with a depth of 700~1100 nm and grain sizes ranging from 50 to 100 nm. Additionally, elongated grains exhibit a gradient distribution along the vertical direction, with grain width increasing from the machined surface towards the interior. This gradient distribution suggests that different regions of the machined surface experience varying

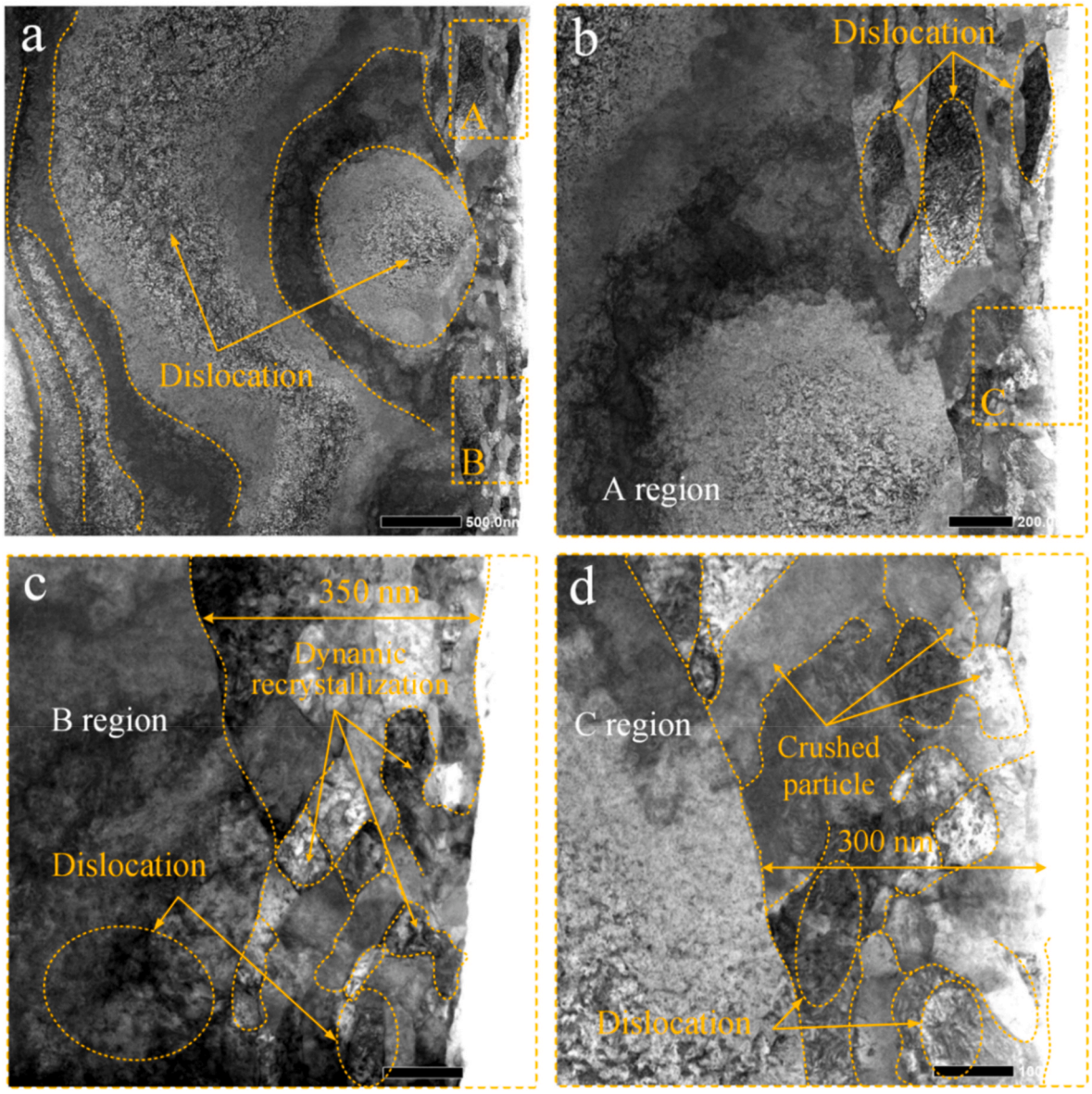


**Fig. 11.** TEM morphologies of machined surface created by CC with various measurement scales: (a) 500 nm, (b) 200 nm, (c–d) 100 nm.

degrees of stress and strain due to the influence of gradient stress fields [29,30]. During UEVC, the cutting load applied by the tool tip facilitates compressive deformation of grains, while ultrasonic vibration enhances the proliferation and interaction of intragranular dislocations. These dislocations subsequently transform into subgrain boundaries. As the cutting process progresses, these subgrain boundaries evolve into grain boundaries, and the compressed grains are refined into nanocrystals through dynamic recrystallization.

Based on the subsurface microstructure, it is reasonable to assume that the first and second deformation zones of the cutting process are also characterised by the presence of a large range of high-density dislocations and nano-fine crystalline layers. This is the key to the inhibition of brittle fracture in UEVC tungsten alloys to generate ductile surfaces.

## 4. Discussion

The high quality of machined surface of tungsten alloys achieved through UEVC is attributed to two primary factors. Firstly, the suppression of tool wear is a consequence of distinctive characteristics of UEVC, including "friction reversal," "tool-work separation," and "reduced cutting forces." Secondly, the inherent "reduction of brittleness and enhancement of toughness" during the cutting process is also a contributing factor [31,32]. Nevertheless, the fundamental mechanism of "reduction of brittleness and enhancement of toughness" in UEVC remains to be fully clarified. Current researches primarily categorize the proposed mechanisms into the "ultrasonic theory", which posits that the ultrasonic vibration involves material modification through ultrasonic-induced dislocation generation and phase transformations [33], and the "elliptical trajectory theory," which asserts that the presence of an elliptical tool trajectory results in a substantially reduced actual cutting depth compared to the nominal cutting depth [34–36]. In addition, including the "high-pressure cutting zone" induced by single-crystal diamond tools and "high-stress peaks" generated by vibrations—are also recognized as critical inhibitors of brittle fracture during tungsten alloys machining. Some researchers even advocate for a synergistic interaction among these mechanisms.

The material removal process in UEVC is shown in Figs. 13(a)–Fig. 13 (b) shows the side view of Fig. 13(a)–and Fig. 13 (b) is further enlarged as Fig. 13(c–d). As shown in Fig. 13 (c), the tool is assumed to

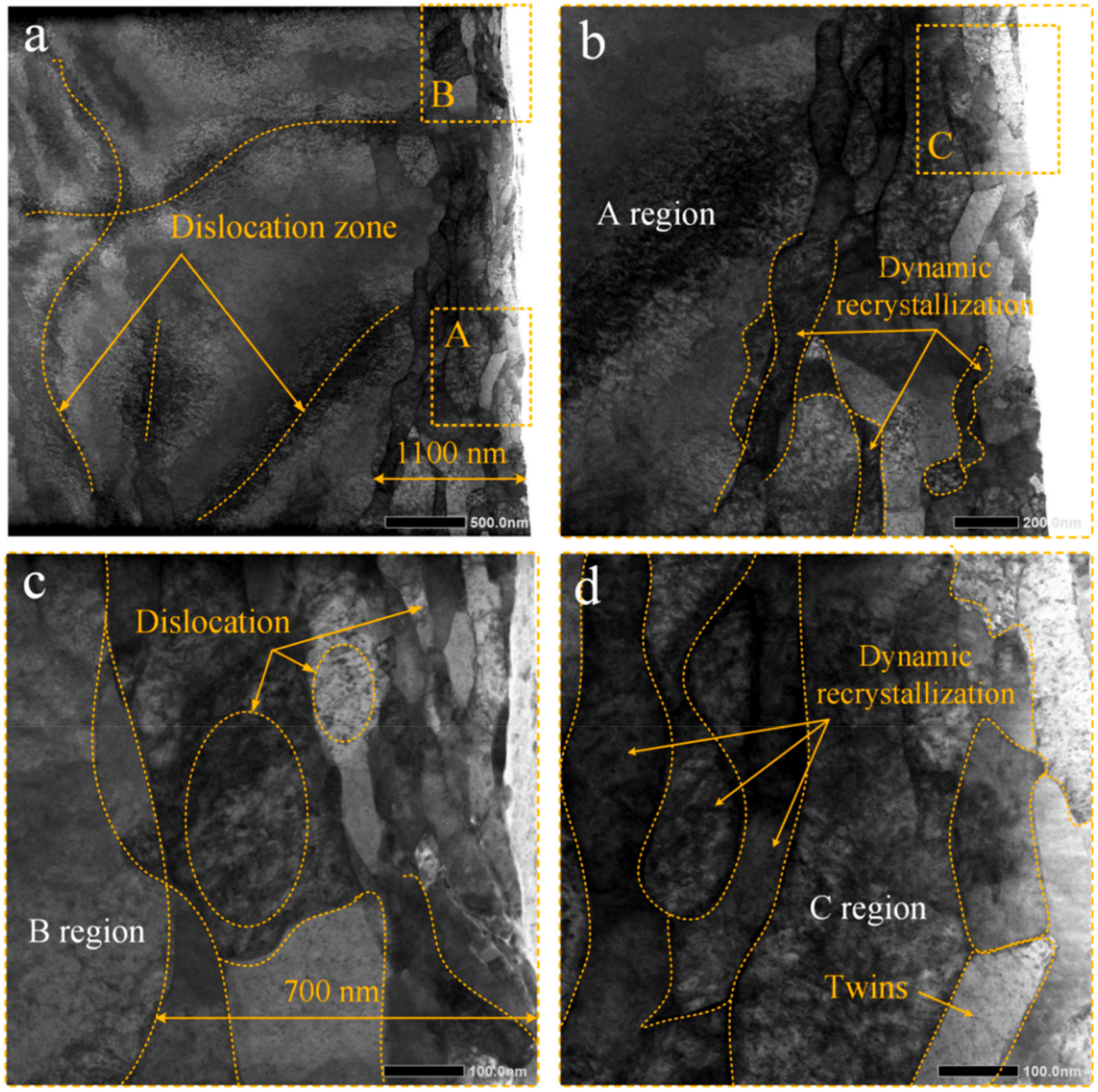


**Fig. 12.** TEM morphologies of machined surface created by UEVC with various measurement scales: (a) 500 nm, (b) 200 nm, (c–d) 100 nm.

be idealized, disregarding the edge radius, and the rake angle is established to 0° to simplify the geometric relationships. At point $t_1$, the tool completes the previous cutting cycle and enters a "tool-workpiece separation" state. At point $t_2$, the tool initiates the subsequent cutting cycle, commencing the removal of a minor amount of material. At point $t_3$, the processing of the transition surface is completed, and subsequently, the current cutting cycle concludes at point $t_4$, where the tool transitions into a "tool-workpiece separation" state. In accordance with the "elliptical trajectory theory", surface generation in UEVC predominantly occurs during the $t_2$-$t_3$ phase. During this interval, the nominal cutting depth is reduced below the critical depth for the brittle-to-ductile transition, enabling plastic removal of the material [21,37].

The afore mentioned theory is undoubtedly applicable to UEVC with natural diamond tools and is widely recognized as the mechanism for achieving plastic deformation-based surface generation in ultra-precision machining. However, it is evidently inapplicable to cemented carbide tools with large edge radius (20–30 μm). As illustrated in Fig. 13 (d), due to the excessively large blunt radius, material removal during $t_2$-$t_3$ interval becomes ineffective (with the peak amplitude of approximately 2 μm, the maximum cutting depth during $t_2$-$t_3$ is limited to 2 μm). Instead, only ironing, extrusion, and friction-induced limited strain occur. inherently negates both elliptical trajectory effects and high-pressure zone formation, thereby enabling the effect of ultrasonic vibration to be verified independently. Material removal primarily occurs during $t_3$-$t_4$ phase, which is defined as the cutting stroke ($l_{cs}$), calculated as the ratio of nominal cutting speed to vibration frequency. This cutting stroke increases with higher nominal cutting speed. Based on experimental characterization, conclude that material removal in tungsten alloys is closely associated with the nucleation and migration of dislocations within the cutting zone.

The nucleation and evolution of dislocations proximate to the crack tip are pivotal in the processes of crack shielding and blunting. Tungsten, as a body-centered cubic (BCC) metal with extremely low dislocation mobility, experiences rapid cleavage fracture of single-crystal tungsten grains when the sliding edge dislocations are insufficient to accommodate the plastic deformation at the crack tip [38,39]. The intrinsic nature of the transition between material brittleness and ductility resides in the competition between the propensity for plastic deformation and crack propagation [40]. The embrittlement tendency inherent in BCC tungsten, resulting from low dislocation activity, can be mitigated by increasing the density of mobile dislocations. Ultrasonic vibration augments the activity and proliferation of dislocation dipoles

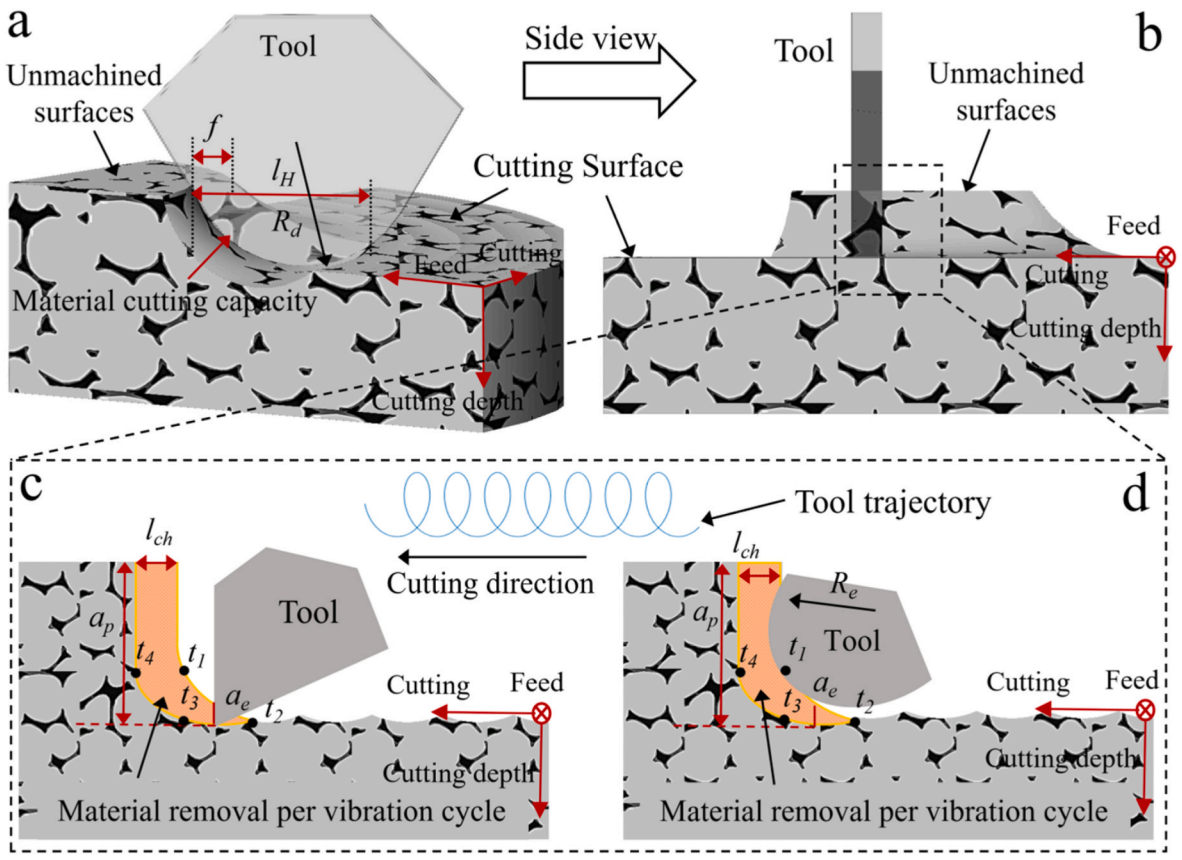


**Fig. 13.** Material removal process of different tools in UEVC: (a) Machining principle of UEVC: (b) Material removal for ideal tool, (c) Material removal for cemented carbide tools.

[16]. In light of this, it is concluded propose that the high-density dislocations induced by UEVC in the primary and secondary deformation zones are crucial in suppressing brittle fracture and achieving ductile surfaces in tungsten alloys. High-density dislocations are further migrated, aggregated and annihilated to generate an ordered ultrafine crystal layer (grain size of approximately 50–100 nm). Although, according to the Hall-Petch relation, grain refinement can increase the yield strength and hardness of a material, which theoretically reduces the machinability, grain refinement can have a significant effect on improving the low-temperature toughness, which has been attributed to the fact that the finer grains can better absorb and dissipate externally loaded energy, allowing the material to maintain a better toughness at low temperatures. Taken together, the presence of the nanofine grain layer is gainful in suppressing brittle fracture during single crystal tungsten processing. So far, high-density dislocations and nano-fine crystalline layers are the intrinsic mechanisms for the improvement of surface quality of UEVC tungsten alloys.

Compared with natural diamond tools in conjunction with UEVC, although the machined surface achieved by cemented carbide tools with UEVC does not reach the ultra-precision machining level. Nonetheless, their economical cost signifies considerable potential for augmenting the batch production of tungsten alloys components. In comparison to CC, the machining-induced dislocation generation and grain refinement facilitate performance-centric manufacturing regulation, including enhanced radiation resistance. In the future, this research endeavors to investigate applications in the fabrication of components that demand moderate machined surface quality but excellent resistance to ion impact, such as the “first wall structures” within fusion devices.

## 5. Conclusions

Experimental investigations were conducted on the precision machining of tungsten alloys (95W-3.5Ni-1.5Fe) using cemented carbide tools in both CC and UEVC to establish the correlation between machined surface quality and subsurface microstructure. Further, the formation mechanism of ductile surface in UEVC of tungsten alloys was analyzed. The main conclusions of this research are as follows:

Compared to CC, UEVC has a significant effect on tool wear. Both of them are mainly mechanical wear, accompanied by other forms of wear such as diffusion wear, oxidation wear, etc. The inhibition of tool wear by UEVC is mainly attributed to the properties of ‘cutting force reduction’ and ‘friction reversal’.

UEVC significantly improves the surface quality of tungsten alloys, which is mainly reflected in the reduction of surface defects and surface roughness (from Sa = 290 nm to Sa = 115 nm). The UEVC process produces much longer chips thanCC (about 3–10 times), which proves the ‘plasticising and brittle reduction’ properties of the UEVC process of tungsten alloys. Sub-surface part: UEVC of tungsten alloys induces a wide range of high-density dislocations on the surface and a uniform, well-organised, ultra-fine-grained sub-surface layer (layer depth of about 1000 nm, particle size of about 50–100 nm), with no visible cracks or other sub-surface damage.These significant improvements are attributed to a shift in the removal mechanism, transitioning from a semi-brittle removal mode, characterized by extensive brittle fractures, to a ductile and semi-ductile mode.

The study ruled out the role of elliptical trajectory, and concluded that the high density of dislocations and nano-fine crystalline layer induced by ultrasonic vibration are the intrinsic mechanism for the improvement of the surface quality of tungsten alloys by UEVC. The positive role of ‘ultrasound’ in the UEVC process is affirmed, which

supports the 'ultrasound theory' in the existing theory.

Finally, due to the low cost of machining tungsten alloys with cemented carbide tools, The UEVC tungsten by cemented carbide tools is considered to be a cutting process with industrial potential for improving the quality and overall performance of large-volume tungsten alloy machining.

## Author contributions

Hao Su: Writing – original draft, Conceptualization, Methodology, Investigation, Data curation, Formal analysis, Validation, Visualization. Zhigang Dong: Supervision, Funding acquisition, writing-reviewing and editing. Yan Bao: Supervision, Validation, Software, writing-reviewing and editing. Renke Kang: Supervision, Project administration, writing and editing. Sen Yin: Software, Methodology, Funding acquisition, Investigation.

## Declaration of competing interest

The authors declare that they have no known competing financial interests or personal relationships that could have appeared to influence the work reported in this paper.

## Acknowledgement

The work described in this paper was partially supported the National Natural Science Foundation of China Joint Fund Integration Program,(U23B6005, National Natural Science Foundation of China, China), China Postdoctoral Science Foundation (2024M750796, China Postdoctoral Science Foundation, China), the Key Research Projects of Higher Education Institutions in Henan Province (24A460010, Henan Provincial Department of Human Resources), the Henan Province Postdoctoral Research Project Funding (351351, Henan Provincial Department of Human Resources, China), the funding support to the State Key Laboratories in Hong Kong from the Innovation and Technology Commission (ITC) of the Government of the Hong Kong Special Administrative Region (HKSAR), China. The authors would also like to express their sincere thanks to the financial support from the Research and Innovation Office of The Hong Kong Polytechnic University.

## References

[1] Song W, Ming X. Present research and future development of tungsten heavy alloys. Rare Met Mater Eng 2012;41.
[2] Ravi Kiran U, Panchal A, Sankaranarayana M, Nageswara Rao GVS, Nandy TK. Effect of alloying addition and microstructural parameters on mechanical properties of 93% tungsten heavy alloys. Mater Sci Eng, A 2015;640:82–90. https://doi.org/10.1016/j.msea.2015.05.046.
[3] Bai J, Xu Z, Zhong W, Wang M, Qian L. On understanding the influence of microstructure on pure tungsten machinability: a micro-end milling case. J Mater Res Technol 2024;33:8435–50. https://doi.org/10.1016/j.jmrt.2024.11.190.
[4] Neu R, Maier H, Balden M, Elgeti S, Gietl H, Greuner H, et al. Investigations on tungsten heavy alloys for use as plasma facing material. Fusion Eng Des 2017;124:450–4. https://doi.org/10.1016/j.fusengdes.2017.01.043.
[5] Li Z, Liu Z, Zhuang Z, Cui Y. Temperature dependent deformation localization in irradiated tungsten. Int J Plast 2021;146:103077. https://doi.org/10.1016/j.ijplas.2021.103077.
[6] Zhang J, Cui T, Ge C, Sui Y, Yang H. Review of micro/nano machining by utilizing elliptical vibration cutting. Int J Mach Tool Manufact 2016;106:109–26. https://doi.org/10.1016/j.ijmachtools.2016.04.008.
[7] Pan Y, Kang R, Dong Z, Du W, Yin S, Bao Y. On-line prediction of ultrasonic elliptical vibration cutting surface roughness of tungsten heavy alloy based on deep learning. J Intell Manuf 2022;33:675–85. https://doi.org/10.1007/s10845-020-01669-9.
[8] Yin S, Dong Z, Kang R, Jin Z, Bao Y. Research on ultrasonic elliptical vibration cutting mechanism of tungsten heavy alloy. SSRN Electron J 2022.
[9] Yin S, Yip WS, Dong Z, Kang R, To S. Experimental and simulation investigation of ultrasonic elliptical vibration cutting of tungsten alloys in ultra-precision machining. J Mater Res Technol 2025;34:77–89. https://doi.org/10.1016/j.jmrt.2024.12.026.
[10] Hao Wang A GYAH, B PZ. Insight into surface formation mechanism during ultrasonic elliptical vibration cutting of tungsten alloy by scratching experiment and molecular dynamics. Tribol Int 2024. https://doi.org/10.1016/j.triboint.2023.109088.
[11] Wang H, Dong Z, Wang C, Kang R, Guo X, Bao Y. Surface/subsurface formation mechanism of tungsten during ultrasonic elliptical vibration cutting. Int J Mech Sci 2024;262:108725. https://doi.org/10.1016/j.ijmecsci.2023.108725.
[12] Wang H, Gao S, Guo X, Ding Y, Kang R. Atomic understanding of the plastic deformation mechanism of 4H-SiC under different grain depth-of-cut during nano-grinding. J Electron Mater 2023;52:4865–77. https://doi.org/10.1007/s11664-023-10457-z.
[13] Dong Z, Wang H, Qi Y, Guo X, Kang R, Bao Y. Effects of minimum uncut chip thickness on tungsten nano-cutting mechanism. Int J Mech Sci 2023;237:107790. https://doi.org/10.1016/j.ijmecsci.2022.107790.
[14] Wang H, Kang R, Bao Y, Wang K, Guo X, Dong Z. Microstructure evolution mechanism of tungsten induced by ultrasonic elliptical vibration cutting at atomic/nano scale. Int J Mech Sci 2023;253:108397. https://doi.org/10.1016/j.ijmecsci.2023.108397.
[15] Wang H, Dong Z, Yuan S, Guo X, Kang R, Bao Y. Effects of tool geometry on tungsten removal behavior during nano-cutting. Int J Mech Sci 2022;225:107384. https://doi.org/10.1016/j.ijmecsci.2022.107384.
[16] Bai J, Xu Z, Qian L. Precision-improving manufacturing produces ordered ultra-fine grained surface layer of tungsten heavy alloy through ultrasonic elliptical vibration cutting. Mater Des 2022;220:110859. https://doi.org/10.1016/j.matdes.2022.110859.
[17] S. S, Priyadarshini A, Chaganti PK, Prabhu G, Mylavarapu P. Effect of machining operations on mechanical properties, surface integrity and corrosion resistance of tungsten heavy alloy. Mater Today Commun 2023;37:106930. https://doi.org/10.1016/j.mtcomm.2023.106930.
[18] Wang Q, Jin Z, Zhao Y, Niu L, Guo J. A comparative study on tool life and wear of uncoated and coated cutting tools in turning of tungsten heavy alloys. Wear 2021;482–483:203929. https://doi.org/10.1016/j.wear.2021.203929.
[19] Olsson M, Bushlya V, Lenrick F, Ståhl J. Evaluation of tool wear mechanisms and tool performance in machining single-phase tungsten. Int J Refract Metals Hard Mater 2021;94:105379. https://doi.org/10.1016/j.ijrmhm.2020.105379.
[20] Nandam SR, Ravikiran U, Rao AA. Machining of tungsten heavy alloy under cryogenic environment. Procedia Materials Science 2014;6:296–303. https://doi.org/10.1016/j.mspro.2014.07.037.
[21] Yanan P, Yan B, Jiajian F, Sen Y, Zhigang D, Renke K. Study on removal mechanism of ultrasonic elliptical vibration cutting of tungsten heavy alloy. J Mech Eng 2023;59:65–74. https://doi.org/10.3901/JME.2023.21.065.
[22] Jiao Z, Kang R, Dong Z, Guo J. Microstructure characterization of W-Ni-Fe heavy alloys with optimized metallographic preparation method. Int J Refract Hard Met 2019;80:114–22. https://doi.org/10.1016/j.ijrmhm.2019.01.011.
[23] Pan Y, Kang R, Bao Y, Yin S, Dong Z. Study on tool wear mechanism of single-crystal diamond in ultrasonic vibration elliptical cutting of tungsten heavy alloy. Wear 2023;516–517:204616. https://doi.org/10.1016/j.wear.2022.204616.
[24] Yang Z, Wang Z, Qin N. Experimental and numerical investigation of model I dynamic fracture toughness of 95W-3.5Ni-1.5Fe alloy using the semi-circular bend specimens. Eng Fract Mech 2021;258:108053. https://doi.org/10.1016/j.engfracmech.2021.108053.
[25] Siu KW, Ngan AHW, Jones IP. New insight on acoustoplasticity – ultrasonic irradiation enhances subgrain formation during deformation. Int J Plast 2011;27:788–800. https://doi.org/10.1016/j.ijplas.2010.09.007.
[26] Wang F, Guo W, Liu J, Li S, Zhou J. Microstructural evolution and grain refinement mechanism of pure tungsten under explosive loading condition. Int J Refract Metals Hard Mater 2014;45:64–70. https://doi.org/10.1016/j.ijrmhm.2014.03.008.
[27] Su H, Shen X, Xu C, He J, Wang B, Su G. Surface characteristics and corrosion behavior of TC11 titanium alloy strengthened by ultrasonic roller burnishing at room and medium temperature. J Mater Res Technol 2020;9:8172–85. https://doi.org/10.1016/j.jmrt.2020.05.059.
[28] Zhao W, He W, Zhu D, Liang X, Pang Z, Song J, et al. Comparative investigation on microstructure and mechanical properties of GH4169 superalloy after laser shock peening with and without coating. J Mater Res Technol 2024;29:276–85. https://doi.org/10.1016/j.jmrt.2024.01.090.
[29] Xing Y, Liu Y, Li Y, Yin T, Li D, Xue C, et al. Inhibiting surface and subsurface damage in ultrasonic vibration-assisted ultraprecision diamond cutting of high-entropy alloy. J Mater Res Technol 2025;34:880–97. https://doi.org/10.1016/j.jmrt.2024.12.124.
[30] Wang YG, Chen X, Wei LL, Misra RDK, Chen J. Interplay between deformation and fracture mechanism in gradient nanostructured austenitic stainless steel. J Mater Res Technol 2024;33:4594–608. https://doi.org/10.1016/j.jmrt.2024.10.149.
[31] Zhang J, Han L, Zhang J, Liu H, Yan Y, Sun T. Brittle-to-ductile transition in elliptical vibration-assisted diamond cutting of reaction-bonded silicon carbide. J Manuf Process 2019;45:670–81. https://doi.org/10.1016/j.jmapro.2019.08.005.
[32] Zhang J, Zhang J, Cui T, Hao Z, Al Zahrani A. Sculpturing of single crystal silicon microstructures by elliptical vibration cutting. J Manuf Process 2017;29:389–98. https://doi.org/10.1016/j.jmapro.2017.09.003.
[33] Siu KW, Ngan AHW, Jones IP. New insight on acoustoplasticity – ultrasonic irradiation enhances subgrain formation during deformation. Int J Plast 2011;27:788–800. https://doi.org/10.1016/j.ijplas.2010.09.007.
[34] Wang J, Yang Y, Guo P. Effects of vibration trajectory on ductile-to-brittle transition in vibration cutting of single crystal silicon using a non-resonant tool. Procedia CIRP 2018;71:289–92. https://doi.org/10.1016/j.procir.2018.05.017.
[35] Zhang X, Arif M, Liu K, Kumar AS, Rahman M. A model to predict the critical undeformed chip thickness in vibration-assisted machining of brittle materials. Int

J Mach Tool Manufact 2013;69:57–66. https://doi.org/10.1016/j.ijmachtools.2013.03.006.
[36] Zhang J, Zhang J, Liu C, Chen X, Xiao J, Xu J. Machinability of single crystal calcium fluoride by applying elliptical vibration diamond cutting. Precis Eng 2020;66:306–14. https://doi.org/10.1016/j.precisioneng.2020.06.008.
[37] Li L, Xu J, Ji M, Yin Y, Chen M. On crack suppression mechanisms of ultrasonic elliptical vibration cutting of 3Y-TZP ceramics. Ceram Int 2022;48:28308–26. https://doi.org/10.1016/j.ceramint.2022.06.138.
[38] Marichal C, Srivastava K, Weygand D, Van Petegem S, Grolimund D, Gumbsch P, et al. Origin of anomalous slip in tungsten. Phys Rev Lett 2014;113. https://doi.org/10.1103/PhysRevLett.113.025501.
[39] Cereceda D, Diehl M, Roters F, Raabe D, Perlado JM, Marian J. Unraveling the temperature dependence of the yield strength in single-crystal tungsten using atomistically-informed crystal plasticity calculations. Int J Plast 2016;78:242–65. https://doi.org/10.1016/j.ijplas.2015.09.002.
[40] Zhang Y, Han W. Mechanism of brittle-to-ductile transition in tungsten under small-punch testing. Acta Mater 2021;220:117332. https://doi.org/10.1016/j.actamat.2021.117332.